HHS Public Access

Author manuscript

Ultrasound Med Biol. Author manuscript; available in PMC 2017 August 01.

Published in final edited form as:

Ultrasound Med Biol. 2016 August ; 42(8): 1890–1902. doi:10.1016/j.ultrasmedbio.2016.03.018.

Non-Invasive Ultrasound Liver Ablation using Histotripsy: Chronic Study in an *in vivo* Rodent Model

Eli Vlaisavljevich[1], **Joan Greve**[1], **Xu Cheng**[2], **Kimberly Ives**[1], **Jiaqi Shi**[3], **Lifang Jin**[4], **Alexa Arvidson**[1], **Tim Hall**[1], **Theodore H. Welling**[5], **Gabe Owens**[1,6], **William Roberts**[1,2], and **Zhen Xu**[1,6]

[1]Department of Biomedical Engineering, University of Michigan, Ann Arbor, MI

[2]Department of Urology, University of Michigan, Ann Arbor, MI

[3]Department of Pathology, University of Michigan, Ann Arbor, MI

[4]Department of Ultrasound, Shanghai Jiaotong University, Shanghai, China

[5]Department of Surgery, University of Michigan, Ann Arbor, MI

[6]Department of Pediatrics and Communicable Diseases, University of Michigan, Ann Arbor, MI

Abstract

Hepatocellular carcinoma (HCC) or liver cancer has the fastest growing incidence among cancers in the United States. Current liver ablation methods are thermal-based and share limitations due to the heat sink effect from the blood flow through the highly vascular liver. Recently, our group has investigated histotripsy as a non-invasive liver cancer ablation method. Histotripsy is a non-thermal ultrasonic ablation method that fractionates tissue through the control of acoustic cavitation. Previous experiments in an *in vivo* porcine model show that histotripsy can create well-confined lesions in the liver through ribcage obstruction without damaging the overlying ribs and other tissues. Histotripsy can also completely fractionate liver tissue surrounding major vessels while preserving the vessels. In this study, we investigate the long-term effects of histotripsy liver ablation in a rodent model. We hypothesize that the fractionated histotripsy lesion will be resorbed by the liver, resulting in effective tissue healing. To test this hypothesis, the livers of 20 healthy rats were treated with histotripsy using an 8-element 1 MHz histotripsy transducer. Rats were euthanized after 0, 3, 7, 14, and 28 days (n=4). *In vivo* and post mortem results showed histotripsy lesions were successfully generated in all 20 rats through the intact abdomen. MRI demonstrated primarily negative contrast on day 0, positive contrast on day 3, and rapid normalization of signal intensity thereafter (i.e. signal amplitude returned to baseline levels seen in healthy liver tissue). Histologically, lesions were completely fractionated into an acellular homogenate. The lesions had

Corresponding Author: Eli Vlaisavljevich, Eli Vlaisavljevich, University of Michigan, Department of Biomedical Engineering, 2200 Bonisteel Blvd, Ann Arbor, MI 48109, USA. Phone: (734) 936-3674, evlaisav@umich.edu.

Disclosure notice: Drs. William Roberts, Tim Hall, Gabe Owens, and Zhen Xu have financial interests and/or other relationship with HistoSonics Inc.

a maximum cross-sectional area of 17.2±1.9 mm^2 and sharp boundaries between the lesion and the healthy surrounding tissue after treatment. As the animals recovered after treatment, the histotripsy tissue homogenate was almost completely replaced by regenerated liver parenchyma, resulting in a small fibrous lesion (<1 mm^2 maximum cross-section) remaining after 28 days. The results of this study suggest that histotripsy has potential as a non-invasive liver ablation method for effective tissue removal.

Keywords

Liver cancer; ultrasound; cavitation; non-invasive tissue ablation; histotripsy

Introduction

More than 700,000 people are diagnosed with liver cancer every year, with 35,660 cases in the US alone in 2015 (ACS 2015). While liver transplantation may be curative, only a small number of patients will receive this treatment as tumors must be within an early stage (single tumor 5 cm or less; 2–3 tumors 3 cm or less). The limited donor availability also greatly constrains the number of liver transplants (El-Serag and Mason 1999; Bosch et al. 2004). Surgical resection of liver tumors is a proven treatment option but is associated with high rates of morbidity and mortality (Livraghi et al. 2011). Further, surgical resection is not possible in many cases such as patients with decompensated cirrhosis (Parikh and Hyman 2007; Livraghi et al. 2011).

One approach to address these issues is the development of local, non-invasive ablation therapies. Currently available minimally or non-invasive ablation methods are mostly thermal based, including radiofrequency ablation (RFA), microwave therapy, cryoablation, laser ablation, and high intensity focused ultrasound (HIFU) (Charnley et al. 1989; ter Haar 2001; Erce and Parks 2003; Head and Dodd 2004; Leslie and Kennedy 2006; Liapi and Geschwind 2007). While these therapies have shown some success, they share inherent limitations due to the heat sink effect from blood flow (Patterson et al. 1998; Curley 2001; Lu et al. 2003; Marrero and Pelletier 2006) as well as the potential for damage to adjacent structures or major biliary radicles. Thermal ablation is inconsistent in tissue with non-uniform heat dissipation patterns, which is common in hypervascular liver tumors (Livraghi et al. 2003). In particular, for tissue near major vessels, thermal ablation often results in incomplete tumor necrosis (Aschoff et al. 2001; Kudo 2010). In addition, these methods are often unsuitable for treating tumors larger than 3 cm due to the excessive treatment time and practical probe sizes (Patterson et al. 1998; Curley 2001; Lu et al. 2003; Marrero and Pelletier 2006).

Recently, our group has developed histotripsy as a potential non-invasive liver cancer ablation method (Vlaisavljevich et al. 2013). Histotripsy is a non-thermal ultrasonic ablation method that fractionates tissue through the control of acoustic cavitation (Xu et al. 2004; Parsons et al. 2006a; Roberts et al. 2006). Since histotripsy is non-thermal, it is not affected by the heat sink effect from blood vessels and does not have the limitations associated with thermal ablation methods such as damage to other structures. Further, the histotripsy

cavitation cloud can be visualized with ultrasound imaging, allowing precise targeting and real-time treatment feedback (Vlaisavljevich et al. 2013). The change in the tissue during treatment can also be directly monitored using standard imaging modalities such as ultrasound and MRI, which allows histotripsy to be guided by real-time imaging (Hall et al. 2007b; Wang et al. 2009; Allen et al. 2012; Allen et al. 2014; Zhang et al. 2015). An initial study by our group demonstrated the feasibility of applying histotripsy *in vivo* for non-invasive liver ablation in a porcine model with similar size and anatomic similarities to its human counterpart (Vlaisavljevich et al. 2013). Histotripsy was capable of creating well-defined lesions at locations throughout the entire liver through ribs and overlying tissue, with the treated liver fractionated into an acellular fluid homogenate with no recognizable cellular structures (Vlaisavljevich et al. 2013). Additionally, histotripsy was shown capable of completely fractionating the liver tissue near the major hepatic blood vessels and gallbladder while preserving these critical hepatic structures, due to the resistance of stiffer tissues to histotripsy-induced tissue damage (Vlaisavljevich et al. 2013; Vlaisavljevich et al. 2014). Finally, a separate porcine study demonstrated that histotripsy can generate lesions in the liver through full ribcage obstruction without inducing any substantial thermal effects or damage to overlying tissues (Kim et al. 2014).

Although previous work has demonstrated the feasibility of using histotripsy for non-invasive liver ablation, these studies have been limited to investigating the acute effects of histotripsy during and immediately following treatment (Vlaisavljevich et al. 2013; Kim et al. 2014). In this study, we investigate the long-term effects of histotripsy liver ablation in a rodent model commonly used for therapeutic development of HCC. The rat model was chosen for these studies rather than a larger animal model to allow for more animals, longer experiment durations, and a lower cost. Based on the previous acute studies showing histotripsy completely fractionates the liver into an acellular liquid homogenate, we hypothesize that the histotripsy lesion will be resorbed by the tissue over time, resulting in effective tissue removal. This hypothesis is supported by previous work studying the chronic response of prostate, kidney, and cardiac tissues treated with histotripsy, which showed histotripsy lesions were absorbed over time leaving only a small scar or an empty void in the treated region (Hall et al. 2007a; Hall et al. 2009; Owens et al. 2012; Kim et al. 2013). In this study, we investigate the chronic response of liver tissue to histotripsy therapy for the first time, including the use of non-invasive MRI imaging technology. Over 28 days after treatment, the histotripsy lesions were characterized using gross morphology, histological analysis, and MRI.

Materials and Methods

All procedures were approved by the University Committee on Use and Care of Animals at the University of Michigan.

Animal Preparation

A total of 20 male Sprague Dawley rats weighing between 290–310 grams were treated with histotripsy. Before histotripsy, the rat abdomen was shaved and treated with a depilatory cream to improve ultrasound coupling. To ensure ultrasound propagation to targeted tissue,

rats were positioned and fastened onto a custom-built animal platform over a tank of degassed water (Fig. 1). A temperature probe was placed into the water tank for continuous monitoring and recording of the water temperature, which was kept at a target temperature of 35–37°C. Rats were induced and then maintained on 1–5% isoflurane in 1 L/min of oxygen (SurgiVet V704001, Smiths Medical, Waukesha, Wisconsin, USA) for the duration of the histotripsy treatment (Fig. 1C). A pulse-oximeter (SurgiVet V3395, Smiths Medical, Waukesha, Wisconsin, USA) was attached to the rat's paw for continuous monitoring and recording of the pulse and oxygenation levels throughout the procedure. In addition, a rectal thermometer was inserted into the rat to continuously measure the rectal temperature.

Prior to applying histotripsy, the desired treatment location was imaged using a 20 MHz imaging transducer (L40-8/12, Ultrasonix, Vancouver, Canada) aligned coaxially with the 8 element 1 MHz 1 MHz histotripsy therapy transducer (Fig. 1B). The focal position of the therapy transducer in the imaging field of view was found prior to therapy by generating a bubble cloud in degassed water and identifying the location of the hyperechoic region. The location of the bubble cloud was marked on the ultrasound imaging screen to indicate the transducer focal position in free field. The rat was then placed above the transducer, and targeting was achieved by aligning the transducer focus to the selected treatment region in the liver. Histotripsy was applied transcutaneously with a portion of the rib cage within the acoustic pathway. After treatment, rats were either euthanized for analysis or recovered for 3, 7, 14, or 28 days (n=4 each). After treatment, recovery animals were given a Carprofen (Rimadyl, Pfizer, NY, NY, USA) analgesic (5 mg/kg) subcutaneously prior to histotripsy therapy and one day after histotripsy therapy. Recovery animals were monitored by a trained veterinarian for five days following treatment and then twice weekly for the duration of the experiment in order to monitor for grooming activity, appetite, indications of pain and activity levels. At the conclusion of the experiments, rats were euthanized with CO_2 administration and the target tissue was harvested for histological evaluation.

Histotripsy Lesion Generation

Histotripsy lesions were generated in the inferior regions of the liver using a custom-built 1 MHz focused ultrasonic transducer designed for small animal experiments (Fig. 1B). To generate histotripsy pulses, a custom high-voltage pulser developed in-house was used to drive the transducers. The pulser was connected to a field-programmable gate array (FPGA) development board (DE0-Nano Terasic Technology, HsinChu, Taiwan) specifically programmed for histotripsy therapy pulsing. This setup allowed the transducers to output short pulses consisting of less than two cycles, which have previously been shown to produce histotripsy bubble clouds when a distinct pressure threshold is achieved inside the tissue (Maxwell et al. 2013; Lin et al. 2014; Vlaisavljevich et al. 2015a; Vlaisavljevich et al. 2015b). The acoustic output of the transducer was measured by a fiber-optic probe hydrophone (FOPH) built in-house (Parsons et al. 2006b), as outlined in previous studies (Maxwell et al. 2013; Lin et al. 2014; Vlaisavljevich et al. 2015a; Vlaisavljevich et al. 2015b). An example acoustic waveform is shown in Figure 2. Histotripsy pulses were applied to the liver at a pulse repetition frequency (PRF) of 100 Hz and an estimated *in situ* peak negative pressure >30 MPa. The acoustic output used for experiments was estimated by a summation of the output focal *p*- values from individual transducer elements since the

waveforms could not be directly measured due to cavitation damaging the FOPH fiber tip. Using this approach, the summed waveform generated an estimated peak negative pressure of 34.5 MPa in free field at the experimental driving amplitudes.

The inferior regions of the rat liver were targeted in this study to minimize the lung tissue exposed to the acoustic field, as previous work has demonstrated that lung hemorrhage can occur at significantly lower acoustic amplitudes (Apfel and Holland 1991; Holland et al. 1996). Histotripsy lesions were generated by mechanically scanning the therapy focus to follow a 4×4 mm square grid inside the rat liver. Each point in the grid was treated for 5 seconds (500 pulses) before the focus was moved to an adjacent spot 0.5 mm apart. The procedure was monitored with ultrasound imaging (Fig. 3A), and pre-treatment and post-treatment ultrasound images of the targeted region were collected for comparison purposes. After treatment, rats were euthanized with CO_2 administration after 0, 3, 7, 14, or 28 days (n=4 each). After euthanizing, the liver and lungs were harvested for histological evaluation.

Magnetic Resonance Imaging (MRI)

Lesion progression of the rats euthanized after 28 days (n=4) was monitored over the course of the experiment with MRI on days 0, 3, 7, 14, and 28. MRI was performed at 7.0 T using a Direct Drive console (Agilent Technologies, Santa Clara, CA, USA). Days 0, 3, and 7 used a 60 mm inner-diameter transmit-receive radiofrequency (RF) volume coil (Morris Instruments, Ontario, Canada) while a 72 mm RF coil (Rapid Biomedical, Rimpar, Germany) was necessary on days 14 and 28 due to animal growth. Animals were anesthetized and maintained on ~2% isoflurane in 1L/min of oxygen. They were placed in the supine position for imaging. Body temperature was monitored and maintained near 37° C using a rectal temperature probe and warm air, while also monitoring respiration (SA Instruments, Stony Brook, NY; Labview, Austin, TX, USA). A high number of excitations was used to compensate for artifacts due to respiratory motion in order to provide the best contrast between normal and treated liver tissue, while maintaining a reasonable imaging time. After pilot scans to confirm positioning, a T2-weighted fast spin-echo sequence was used to visualize the liver in the coronal plane. The MRI parameters were a field of view of $(60\ mm)^2$, slice thickness of 1 mm, matrix 256^2 zero-filled to 512^2, repetition time of 2000 ms, echo spacing of 10 ms, echo train length of 8, effective echo time of 20 ms, 16 excitations, and an acquisition time of ~17 min. Images were analyzed using MRVision (Winchester, MA, USA). Manual tracing was used to quantify the area of the histotripsy lesion on each slice, multiplying by slice thickness to get volumetric measurements (mean ± standard deviation). When lung tissue was visible, the distance of the histotripsy lesion from the inferior lobes of the lungs was quantified using manual methods. Statistical comparisons were made using a Student's t-test. P-values<0.05 were considered significant. Error bars on graphs represent standard error of the mean (SEM). Quantification of MRI data was performed without knowledge of histological results (J.M.G).

Morphological and Histological Evaluation

Treated rat liver and overlying lung samples were harvested after experiments and fixed in 10% buffered formalin (Fisher Scientific). After fixing the tissue, the lesion gross morphology was examined prior to histological analysis. Samples were then stained with

hematoxylin and eosin (H&E) and examined under a microscope (Nikon Eclipse 50i) using 4x, 10x, 20x, and 40x objective lenses. The size of the histotripsy lesions in the liver was quantitatively assessed before and after tissue fixing by measuring the maximum cross-sectional area of the histotripsy lesion. As the histotripsy lesions contained regions containing hematoma or granulation tissue, the size of these regions were also quantified for all liver samples, with the results compared for animals euthanized after each time point. The reported values for the maximum cross-sectional area of the histotripsy lesions were taken after tissue fixing to allow for better differentiation of the regions containing the hematoma and granulation tissue, respectively. Although the lesion size slightly decreased during fixing, this change was <3% for all samples. Statistical comparisons were made using a Student's t-test. P-values<0.05 were considered significant. Error bars on graphs represent standard error of the mean (SEM).

Results

Histotripsy Liver Lesion Formation

Histotripsy therapy was applied to the livers of 20 rats through the intact abdomen. A bubble cloud was successfully generated in the livers of all 20 rats and visualized as a hyperechoic zone on ultrasound imaging allowing for real-time treatment monitoring (Fig. 3A). The maximum liver motion due to respiration observed during treatment was ~1mm in the direction of the transducer axis. The bubble cloud was observed to remain confined inside the treatment region and did not appear to be affected by the small amount of respiratory motion. After treatment, the fractionated tissue was observed as a hypoechoic zone on ultrasound imaging due to the reduced size and density of the sound scatterers present in the fractionated zone and primarily negative contrast on MRI (Fig. 3B), as seen in previous studies (Wang et al. 2009; Vlaisavljevich et al. 2013; Kim et al. 2014). For the acute group (n=4), the rats were euthanized within one hour after the application of histotripsy, and the liver was harvested for gross morphology (Fig. 3C) and histological analysis (Fig. 3D). Histological evaluation of histotripsy liver lesions showed complete fractionation of hepatic parenchyma inside the treated volume, with sharp boundaries of <50–100 μm between intact and completely fractionated tissue (Fig. 3D). Localized hemorrhage was observed inside the acute lesions, but no hemorrhage was observed in the surrounding intact liver tissue.

Overlying tissues in the acoustic path were examined after treatment for signs of potential damage. Gross morphological examination showed no signs of damage to overlying skin, muscle, or ribs. However, localized hemorrhage was observed after treatment in the inferior regions of the lungs, which were in the acoustic path (Fig. 3E,F). In the rats that showed the most significant lung hemorrhage, the SpO_2 was observed to decrease from >95% to ~80% during the treatment before recovering to normal levels after treatment. No hemorrhage was observed in the superior regions of the lung, likely because these regions were not exposed to the acoustic field. The fluctuation of the heart rate and respiration rate during treatment was maintained within ±10% of the baseline values observed before treatment. The core body temperature did not drop more than 1°C throughout the duration of the treatment.

Histotripsy Chronic Lesion Progression

The chronic response to histotripsy liver ablation was assessed for a period of 28 days. After recovery from non-invasive ultrasound surgery, rats were observed to return to normal behavior (i.e. moving around in the cage) within 30 minutes of treatment. No change in general behavior was observed in the rats during the course of the 28 days. More specifically, no animals became hunched or scruffy, had inappetence, or had a reduction in physical activity during any of the observations. The rat urine appeared slightly pink for approximately one week after treatment, potentially a sign of acute rhabdomyolysis and/or hemoglobinuria, but returned to normal for the duration of the experiment. For the acute rats, histotripsy treated lesions were completely fractionated, with no recognizable cellular structures within the treatment region. The boundaries between the surrounding healthy liver tissue and the completely fractionated homogenate were sharply demarcated (Fig. 4A). The average maximum cross-sectional area of the lesions (n=4) was 17.2±1.9 mm^2, which closely matched the 4 × 4 mm treatment grid and the finite size of the bubble cloud. Histological analysis demonstrated that the histotripsy homogenate at day 0 consisted of mainly red blood cells and fibrin with a few scattered white blood cells (i.e. hematoma) (Fig. 5A,F). From day 3 to day 28, gross analysis of the liver demonstrated that the tissue homogenate (i.e. hematoma) inside the lesions was gradually replaced by regenerated liver parenchyma and scar (Fig. 4). The size of the hematoma was observed to significantly decrease after 3 and 7 days, with no hematoma remaining after 14 and 28 days (Fig. 6). Microscopically, at day 3, foci of fibroblasts started to grow into the histotripsy lesion from the interface between normal liver parenchyma and hematoma together with infiltration of inflammatory cells, mainly neutrophils, lymphocytes, and macrophages (i.e. organizing) (Fig. 5B,G). Additionally, there were also foci of small bile ductular proliferation at the interface, indicating a liver regenerative process in response to injury (Fig. 5G). At day 7, this ingrowth of fibroblasts was more prominent and the major inflammatory component switched to macrophages with foci of foamy macrophages and multinucleated giant cells with calcified debris in their cytoplasm, suggesting that they are the main force of cleaning up the necrotic debris (Fig. 5C,H). In addition, there was an increased bile ductular proliferation at the interface with markedly proliferating hepatocytes at the edge of the lesion, indicated by increased mitotic figures. These findings are indicative of ongoing hepatocellular regeneration in response to the loss of liver parenchyma. By day 14, the lesion was significantly reduced in volume with only a small focus of fibrin (Fig. 5D,I). The majority of the lesion was replaced by normal liver parenchyma and a much smaller focus of foreign body giant cells, hemosiderin-laden macrophages, fibroblasts, scar, and other inflammatory cells. Some of the bile ductules start to grow into the center of the lesion. By day 28, the lesion was mainly replaced by normal liver parenchyma with a minute focus of residual collagenous scar, hemosiderin-laden macrophages, and foreign body giant cells with undigested calcified debris in the cytoplasm (Fig. 4E,J). The organizing granulation tissue maximized after 3 days and decreased after 7 days, which corresponded to a decrease in the total lesion size (Fig. 6). The lesion size continued to decrease over the course of the experiment, resulting in small lesions with an average maximum cross-sectional area of <1 mm^2 after 28 days (n=4) (Fig. 6). There was no significant portal or lobular inflammation, single or confluent liver cell necrosis, fibrosis, or other pathological changes in the surrounding or distant liver parenchyma (Fig. 5K–O).

MRI Liver Lesion Monitoring

In addition to morphological and histological analysis, lesion progression of the rats euthanized after 28 days was monitored with *in vivo* MRI over the course of the experiment. MRI was performed on days 0, 3, 7, 14, and 28. Animals tolerated MRI well at all time points, including only hours after histotripsy treatment on day 0. This was evident based on consistent body temperatures and respiration rates at all imaging time points (36.7±0.3°C, 62±5.5 breaths/min). In addition, qualitatively, other overt signs of distress were absent (i.e. there was minimal or no porphyrin staining, unkempt fur, or hunched position initially, nor did these markers increase during the study). For time points where histotripsy lesions were visible on MRI (typically days 0, 3, and 7; only one lesion was visible at day 14), signal intensity was heterogeneous across the lesion. However, MRI consistently demonstrated primarily negative contrast on day 0 and positive contrast on day 3 (Fig. 7). Such changes in signal intensity imply extracellular/extravasated blood products containing iron and edema were the dominant influence on the MRI signal after day 0 and day 3, respectively. There was a rapid normalization of signal intensity thereafter, with no visible lesions observed at day 28. A thin dark line circumscribing the lesion along portions of its perimeter was observed in a number of images, typically days 3 and 7, implying either a higher concentration of blood products or a highly structured material. The evolution of total lesion volume by MRI demonstrated an average lesion volume of 279.2±233.2 mm^3, 267.9±103.4 mm^3, 71.5±60.0 mm^3, 19.3±38.6 mm^3, and 0±0 mm^3 after days 0, 3, 7, 14, and 28, respectively (Fig. 8). Although not every dataset included lungs in the same field of view as the liver lesions, for those that did, the average distance between the superior edge of the lesions and the inferior surface of the lungs was 18.0±2 mm.

Lung Histological Analysis

Due to the limitations with the small animal model, the acoustic path passed though the inferior lobes of the lung, resulting in local hemorrhage in these regions following histotripsy therapy (Fig. 3E). Histological analysis of the effected regions of the lung (i.e. regions with hemorrhage observed on gross morphology) demonstrated infiltrating red blood cells throughout the alveolar space after treatment (Fig. 9A,F). This diffuse hemorrhage was only observed in the inferior lobes of the lung and was likely caused by cavitation damage rupturing small blood vessels, as previous work has demonstrated a significantly reduced cavitation threshold for lung tissue due to the presence of air (Apfel and Holland 1991; Holland et al. 1996). The larger blood vessels in the effected regions of the lung were observed to remain intact, similar to previous studies demonstrating large vessels are more resistant to histotripsy damage due to the increased tissue stiffness (Vlaisavljevich et al. 2013; Vlaisavljevich et al. 2014). After recovery from therapy, the number of red blood cells inside the alveolar space was observed to steadily decrease, with minimal hemorrhage remaining after 28 days (Fig. 9). In addition to the clearance of red blood cells, an acute immune response was observed, with local infiltration of leukocytes, macrophages, and fibroblasts observed after 3 days. The interstitial tissue surrounding the alveolar walls in the effected regions was observed to thicken over time (Fig. 9). After day 28, histological analysis demonstrated nearly normal lung tissue with open alveolar space (Fig. 9E) and only a few regions of thickened alveolar walls (Fig. 9J).

Discussion

In this study, we investigated the effects of histotripsy liver ablation in a chronic rat model. Well-confined bubble clouds were generated in the livers of all 20 rats, resulting in the formation of completely fractionated histotripsy lesions with sharply demarcated boundaries between the surrounding healthy liver tissue and the lesion. These well-defined lesions are a result of the mechanical ablation process underlying histotripsy and closely match previous studies showing lesions with more sharply demarcated boundaries for mechanical tissue ablation (i.e. histotripsy and boiling histotripsy) in comparison to thermal lesions (Parsons et al. 2006a; Roberts et al. 2006; Vlaisavljevich et al. 2013; Wang et al. 2013; Khokhlova et al. 2014; Schade et al. 2014; Schade et al. 2015). Immediately after treatment, the histotripsy lesion consisted of acellular debris, fibrin, and red blood cells that accumulated inside the lesion due to local injury and hemorrhage. As the animals recovered over the course of 28 days, the homogenate within the histotripsy lesion was gradually replaced by regenerated liver parenchyma, granulation tissue, scar, and macrophages, characteristic of a typical wound healing response in the liver. After 28 days, the histotripsy lesions were almost completely replaced by regenerated hepatocytes, with only a small focus of scar and residual foreign body giant cells cleaning up the calcified debris remaining (<1 mm^2 maximum cross-section). It is possible that this lesion would have been further resorbed over longer time points if the experiment would have been continued beyond day 28.

The results of this study are promising for the development of histotripsy as a non-invasive ablation modality for the treatment of liver cancer. The nearly complete resorption of the histotripsy lesions, as observed in this study after 28 days, demonstrates that histotripsy not only causes cell death to the target tissue by completely fractionating the tissue into an acellular homogenate, but also effectively removes the targeted tissue from the liver over time. If a similar healing response occurs in a clinical setting, then this would be a major advantage for histotripsy therapy compared to thermal ablation methods in which the tissue is destroyed by thermal necrosis, often leaving behind a permanent fibrotic scar (Coad et al. 2003; Marrero and Pelletier 2006; Ding et al. 2013). For example, a post-liver transplant histopathologic study of HCC lesions treated with RFA has shown “thermally fixed” lesions remaining 14 months after treatment (Coad et al. 2003). In addition, the fibrotic masses left behind after thermal ablation are associated with negative side effects such as pain or loss of liver function due to the displaced volume of healthy liver tissue, while also making it difficult to identify residual or recurrent tumor tissue. As such, thermal ablation methods are often used in conjunction with surgery, with the necrotic fibrous tissue requiring subsequent removal via invasive surgery. In contrast, the results of this study suggest that histotripsy has the potential to completely ablate liver tumors into an acellular homogenate that will be replaced by normal liver parenchyma over time. It appears that the acute immune response to the histotripsy treatment contributes to the organization of the lesion starting from the interface, leaving only a very small scar in the region of the liver previously treated with histotripsy. Furthermore, it should be noted that, although the liver parenchyma contracted around the histotripsy lesions due to scar formation, there was no evidence of damage to the surrounding liver parenchyma. No necrosis, significant portal or lobular inflammation, or other pathology was identified in the surrounding liver parenchyma. While this study

investigated the chronic effects of histotripsy liver ablation in a healthy liver model, we hypothesize that a fractionated liver tumor homogenate would be similarly resorbed by the tissue after treatment with histotripsy, similar to previous studies investigating histotripsy for the treatment of renal and prostate tumors (Styn et al. 2010; Schade et al. 2012). Future work is ongoing to investigate the long-term effects of histotripsy liver cancer ablation in a chronic liver cancer model.

In addition to the detailed assessment of lesion evolution using ultrasound imaging, gross morphology, and histology, this study used MRI to assess the progression of the histotripsy lesion over time. To our knowledge, this is the first time a histotripsy lesion has been observed on MRI in an *in vivo* setting for acute or chronic assessment. Given that the MRI signal is a macroscopic representation of the microscopic tissue environment, first time application of *in vivo* MRI must be validated using *ex vivo* methods such as morphology and histology. The *in vivo* MRI results were consistent with *ex vivo* endpoints in this study. The negative contrast seen on day 0 is congruent with the hematoma and extravasated blood products visualized via morphology and histology. These features are likely to contain red blood cells and hemoglobin in various oxygenated states which would reduce the T2 time constant, resulting in a lower signal intensity (Queiroz-Andrade et al. 2009). Similarly, as seen on day 3, initial resorption of the hematoma temporarily increases fluid content (i.e. edema) which would lead to an increase in the T2 time constant and higher signal intensity (Chundru et al. 2014). The remaining hematoma and replacement granulation tissue, as seen on days 7–14, would lead to a residual, localized low signal intensity (Ng et al. 2015). Finally, as the lesion is resolved, the MRI signal returns to being iso-intense. The trends in lesion size were also consistent between MRI and *ex vivo* endpoints, with the decrease in lesion volume over time measured by MRI matching the trend of decreasing cross-sectional area observed on gross morphology and histology.

The finding that MRI can be used to clearly visualize histotripsy liver lesions after treatment, acutely and chronically, using a standard MRI sequence may be a significant advantage for histotripsy, allowing for the treatment effect to be monitored immediately following therapy. The immediate histotripsy treatment feedback would be a significant improvement over thermal ablation or drug therapies, in which the effectiveness of the treatment often cannot be assessed until a few weeks or months after application (Coad et al. 2003; Marrero and Pelletier 2006). The immediate treatment feedback on MRI is a result of the mechanical breakdown of the tissue structures at the focus, as has been established in previous studies investigating MRI imaging of lesions generated using acoustic cavitation-based tissue ablation (Allen et al. 2012; Alkins et al. 2013; Kim et al. 2013; Vlaisavljevich et al. 2013; Kim et al. 2014; Partanen et al. 2014). In addition to this immediate treatment feedback, the ability to quantify the changes in total lesion volume after recovery from treatment, as demonstrated in this study, would be a major benefit. If the large changes in T2 signal intensity and the rapid resolution of the lesion (~2 weeks) are the same in liver cancer patients, one might expect the remaining tumor to vary in intensity with respect to the healthy liver tissue, while the ablated tissue would be isointense as seen in this work, allowing for the identification of residual or untreated tumor tissue after treatment. However, it is also possible that the fibrous tissue circumscribing the lesion, which results in localized constriction at later time points, may be challenging to visualize in a clinical setting due to

resolution limitations, respiratory motion, or surrounding tissues (such as the gastro-intestinal organs) back-filling space left by the contracted liver tissue. As a result, future work will investigate the use of alternative imaging sequences or contrast agents in order to optimally differentiate healthy liver tissue, tumor tissue, and the fractionated histotripsy tissue homogenate.

While the results of this study demonstrated that histotripsy liver ablation was well tolerated by the animals during and after treatment (i.e. stable vital signs during treatment and no change in animal behavior after treatment), the results suggest that histotripsy transducers should be designed to avoid the presence of lungs in the acoustic field in order to prevent the lung hemorrhage observed in this study. Previous work has shown a significant decrease in the cavitation threshold in lung tissue due to the gas content, which increases the likelihood of generating cavitation even at the reduce pressures outside the histotripsy focus. While it is promising that the lung damage observed in this study appeared to be reversible over time, this lung damage has the potential to be fatal during treatment if the extent of the damage is too severe as was observed in two preliminary experiments targeting the upper lobes of the liver in which the entire lungs were exposed to the acoustic field. As such, it is important to design histotripsy transducers with the proper acoustic window in order to avoid the passage of sound through the lungs. In our previous study in an *in vivo* porcine model, histotripsy was shown capable of targeting every region of the liver without inducing any lung hemorrhage (Vlaisavljevich et al. 2013; Kim et al. 2014). Due to the limitations of the small animal model used in this study, a transducer with a larger acoustic path (with respect to the animal) was required in order to generate the high pressures required for histotripsy. While the lung hemorrhage observed in this study is a limitation of the small animal model, the results nonetheless highlight the need for histotripsy transducer designs that minimize sound propagation through the lungs.

Conclusions

This study investigated the effects of histotripsy liver ablation in a chronic rat model. Histotripsy was capable of creating lesions within the liver through the intact abdomen in all animals, and the lesions were observed to be mostly replaced by regenerated liver parenchyma over the course of the 28 day experiment. The finding that histotripsy can be used to non-invasively ablate regions of the liver, resulting in the effective removal of the tissue over time, demonstrates a major advantage of histotripsy therapy compared to thermal ablation techniques that ablate the tissue by thermal necrosis, thereby leaving a chronic fibrous mass of scar tissue inside the liver. Overall, the results of this study suggest that histotripsy has potential as a non-invasive liver cancer ablation method for effective tissue removal.

Acknowledgments

This material is based upon work supported by a National Science Foundation Graduate Research Fellowship for Eli Vlaisavljevich. This work was supported by grants from National Institute of Biomedical Imaging And Bioengineering (NIBIB) of the National Institutes of Health under Award Number R01EB008998, a Research Scholar Grant from the American Cancer Society (RSG-13-101-01-CCE), the Hartwell Foundation, and the Focused Ultrasound Foundation.

References

ACS. Cancer Facts and Figures 2015. American Cancer Society; 2015.

Alkins R, Huang Y, Pajek D, Hynynen K. Cavitation-based third ventriculostomy using MRI-guided focused ultrasound. J Neurosurg. 2013; 119:1520–9. [PubMed: 24074494]

Allen SP, Hall TL, Cain CA, Hernandez-Garcia L. Controlling cavitation-based image contrast in focused ultrasound histotripsy surgery. Magn Reson Med. 2014

Apfel RE, Holland CK. Gauging the likelihood of cavitation from short-pulse, low-duty cycle diagnostic ultrasound. Ultrasound Med Biol. 1991; 17:179–85. [PubMed: 2053214]

Aschoff AJ, Merkle EM, Wong V, Zhang Q, Mendez MM, Duerk JL, Lewin JS. How does alteration of hepatic blood flow affect liver perfusion and radiofrequency-induced thermal lesion size in rabbit liver? J Magn Reson Imaging. 2001; 13:57–63. [PubMed: 11169804]

Bosch FX, Ribes J, Diaz M, Cleries R. Primary liver cancer: worldwide incidence and trends. Gastroenterology. 2004; 127:S5–S16. [PubMed: 15508102]

Charnley RM, Doran J, Morris DL. Cryotherapy for liver metastases: a new approach. Br J Surg. 1989; 76:1040–1. [PubMed: 2688795]

Chundru S, Kalb B, Arif-Tiwari H, Sharma P, Costello J, Martin DR. MRI of diffuse liver disease: characteristics of acute and chronic diseases. Diagn Interv Radiol. 2014; 20:200–8. [PubMed: 24808418]

Coad JE, Kosari K, Humar A, Sielaff TD. Radiofrequency ablation causes ‘thermal fixation’ of hepatocellular carcinoma: a post-liver transplant histopathologic study. Clin Transplant. 2003; 17:377–84. [PubMed: 12868996]

Curley SA. Radiofrequency ablation of malignant liver tumors. Oncologist. 2001; 6:14–23. [PubMed: 11161225]

Ding J, Jing X, Liu J, Wang Y, Wang F, Du Z. Comparison of two different thermal techniques for the treatment of hepatocellular carcinoma. Eur J Radiol. 2013; 82:1379–84. [PubMed: 23726122]

El-Serag HB, Mason AC. Rising incidence of hepatocellular carcinoma in the United States. N Engl J Med. 1999; 340:745–50. [PubMed: 10072408]

Erce C, Parks RW. Interstitial ablative techniques for hepatic tumours. Br J Surg. 2003; 90:272–89. [PubMed: 12594662]

Hall TL, Hempel CR, Wojno K, Xu Z, Cain CA, Roberts WW. Histotripsy of the prostate: dose effects in a chronic canine model. Urology. 2009; 74:932–7. [PubMed: 19628261]

Hall TL, Kieran K, Ives K, Fowlkes JB, Cain CA, Roberts WW. Histotripsy of rabbit renal tissue in vivo: temporal histologic trends. Journal of Endourology. 2007a; 21:1159–66. [PubMed: 17949317]

Head HW, Dodd GD 3rd. Thermal ablation for hepatocellular carcinoma. Gastroenterology. 2004; 127:S167–78. [PubMed: 15508081]

Holland CK, Deng CX, Apfel RE, Alderman JL, Fernandez LA, Taylor KJ. Direct evidence of cavitation in vivo from diagnostic ultrasound. Ultrasound Med Biol. 1996; 22:917–25. [PubMed: 8923710]

Khokhlova TD, Wang YN, Simon JC, Cunitz BW, Starr F, Paun M, Crum LA, Bailey MR, Khokhlova VA. Ultrasound-guided tissue fractionation by high intensity focused ultrasound in an in vivo porcine liver model. Proc Natl Acad Sci U S A. 2014; 111:8161–6. [PubMed: 24843132]

Kim Y, Fifer CG, Gelehrter SK, Owens GE, Berman DR, Vlaisavljevich E, Allen SP, Ladino-Torres MF, Xu Z. Developmental impact and lesion maturation of histotripsy-mediated non-invasive tissue ablation in a fetal sheep model. Ultrasound Med Biol. 2013; 39:1047–55. [PubMed: 23453378]

Kim Y, Vlaisavljevich E, Owens GE, Allen SP, Cain CA, Xu Z. In vivo transcostal histotripsy therapy without aberration correction. Phys Med Biol. 2014; 59:2553–68. [PubMed: 24785433]

Kudo M. Radiofrequency ablation for hepatocellular carcinoma: updated review in 2010. Oncology. 2010; 78(Suppl 1):113–24. [PubMed: 20616593]

Leslie TA, Kennedy JE. High-intensity focused ultrasound principles, current uses, and potential for the future. Ultrasound Q. 2006; 22:263–72. [PubMed: 17146334]

Liapi E, Geschwind JF. Transcatheter and ablative therapeutic approaches for solid malignancies. J Clin Oncol. 2007; 25:978–86. [PubMed: 17350947]

Lin KW, Kim Y, Maxwell AD, Wang TY, Hall TL, Xu Z, Fowlkes JB, Cain CA. Histotripsy beyond the intrinsic cavitation threshold using very short ultrasound pulses: microtripsy. IEEE Trans Ultrason Ferroelectr Freq Control. 2014; 61:251–65. [PubMed: 24474132]

Livraghi T, Makisalo H, Line PD. Treatment options in hepatocellular carcinoma today. Scand J Surg. 2011; 100:22–9. [PubMed: 21482502]

Livraghi T, Solbiati L, Meloni MF, Gazelle GS, Halpern EF, Goldberg SN. Treatment of focal liver tumors with percutaneous radio-frequency ablation: complications encountered in a multicenter study. Radiology. 2003; 226:441–51. [PubMed: 12563138]

Lu DS, Raman SS, Limanond P, Aziz D, Economou J, Busuttil R, Sayre J. Influence of large peritumoral vessels on outcome of radiofrequency ablation of liver tumors. J Vasc Interv Radiol. 2003; 14:1267–74. [PubMed: 14551273]

Marrero JA, Pelletier S. Hepatocellular carcinoma. Clin Liver Dis. 2006; 10:339–51. ix. [PubMed: 16971265]

Maxwell AD, Cain CA, Hall TL, Fowlkes JB, Xu Z. Probability of cavitation for single ultrasound pulses applied to tissues and tissue-mimicking materials. Ultrasound Med Biol. 2013; 39:449–65. [PubMed: 23380152]

Ng E, Tandon AA, Ho BC, Chong BK. Characterising benign fibrous soft-tissue tumours in adults: why is it so difficult and what do we need to know? Clin Radiol. 2015

Owens GE, Miller RM, Owens ST, Swanson SD, Ives K, Ensing G, Gordon D, Xu Z. Intermediate-term effects of intracardiac communications created noninvasively by therapeutic ultrasound (histotripsy) in a porcine model. Pediatr Cardiol. 2012; 33:83–9. [PubMed: 21910018]

Parikh S, Hyman D. Hepatocellular cancer: a guide for the internist. Am J Med. 2007; 120:194–202. [PubMed: 17349437]

Parsons JE, Cain CA, Abrams GD, Fowlkes JB. Pulsed cavitational ultrasound therapy for controlled tissue homogenization. Ultrasound in Medicine and Biology. 2006a; 32:115–29. [PubMed: 16364803]

Parsons JE, Cain CA, Fowlkes JB. Cost-effective assembly of a basic fiber-optic hydrophone for measurement of high-amplitude therapeutic ultrasound fields. J Acoust Soc Am. 2006b; 119:1432–40. [PubMed: 16583887]

Partanen, A.; Farr, N.; Kreider, W.; Khokholova, T.; Maxwell, A.; Wang, Y.; Bailey, M.; Khokholova, V. Use of MRI to visualize mechanically fractionated lesions generated by boiling histotripsy in tissue. Abstract Book of 14th International Symposium for Therapeutic Ultrasound; 2014.

Patterson EJ, Scudamore CH, Owen DA, Nagy AG, Buczkowski AK. Radiofrequency ablation of porcine liver in vivo: effects of blood flow and treatment time on lesion size. Ann Surg. 1998; 227:559–65. [PubMed: 9563546]

Queiroz-Andrade M, Blasbalg R, Ortega CD, Rodstein MA, Baroni RH, Rocha MS, Cerri GG. MR imaging findings of iron overload. Radiographics. 2009; 29:1575–89. [PubMed: 19959509]

Roberts WW, Hall TL, Ives K, Wolf JS Jr, Fowlkes JB, Cain CA. Pulsed cavitational ultrasound: a noninvasive technology for controlled tissue ablation (histotripsy) in the rabbit kidney. J Urol. 2006; 175:734–8. [PubMed: 16407041]

Schade GR, Keller J, Ives K, Cheng X, Rosol TJ, Keller E, Roberts WW. Histotripsy Focal Ablation of Implanted Prostate Tumor in an ACE-1 Canine Cancer Model. Journal of Urology. 2012; 188:1957–64. [PubMed: 22999534]

Schade GR, Maxwell AD, Khokhlova T, Wang Y-N, Sapoznikov O, Bailey MR, Khokhlova V. Boiling histotripsy of the kidney: Preliminary studies and predictors of treatment effectiveness. The Journal of the Acoustical Society of America. 2014; 136:2251.

Schade GR, Wang YN, D'Andrea S, Hwang JH, Lin DW, Bailey MR, Khokhlova TD. Boiling Histotripsy Ablation of in Vivo Renal Carcinoma in the Eker Rat. J Urology. 2015; 193:E459–E60.

Styn NR, Wheat JC, Hall TL, Roberts WW. Histotripsy of VX-2 Tumor Implanted in a Renal Rabbit Model. Journal of Endourology. 2010; 24:1145–50. [PubMed: 20575696]

ter Haar G. High intensity ultrasound. Semin Laparosc Surg. 2001; 8:77–89. [PubMed: 11337740]

Vlaisavljevich E, Kim Y, Allen S, Owens G, Pelletier S, Cain C, Ives K, Xu Z. Image-guided non-invasive ultrasound liver ablation using histotripsy: feasibility study in an in vivo porcine model. Ultrasound Med Biol. 2013; 39:1398–409. [PubMed: 23683406]

Vlaisavljevich E, Kim Y, Owens G, Roberts W, Cain C, Xu Z. Effects of tissue mechanical properties on susceptibility to histotripsy-induced tissue damage. Phys Med Biol. 2014; 59:253–70. [PubMed: 24351722]

Vlaisavljevich E, Lin KW, Maxwell A, Warnez MT, Mancia L, Singh R, Putnam AJ, Fowlkes B, Johnsen E, Cain C, Xu Z. Effects of Ultrasound Frequency and Tissue Stiffness on the Histotripsy Intrinsic Threshold for Cavitation. Ultrasound Med Biol. 2015a

Vlaisavljevich E, Lin KW, Warnez MT, Singh R, Mancia L, Putnam AJ, Johnsen E, Cain C, Xu Z. Effects of tissue stiffness, ultrasound frequency, and pressure on histotripsy-induced cavitation bubble behavior. Phys Med Biol. 2015b; 60:2271–92. [PubMed: 25715732]

Wang TY, Xu Z, Winterroth F, Hall TL, Fowlkes JB, Rothman ED, Roberts WW, Cain CA. Quantitative ultrasound backscatter for pulsed cavitational ultrasound therapy- histotripsy. IEEE Trans Ultrason Ferroelectr Freq Control. 2009; 56:995–1005. [PubMed: 19750596]

Wang YN, Khokhlova T, Bailey M, Hwang JH, Khokhlova V. Histological and biochemical analysis of mechanical and thermal bioeffects in boiling histotripsy lesions induced by high intensity focused ultrasound. Ultrasound Med Biol. 2013; 39:424–38. [PubMed: 23312958]

Xu Z, Ludomirsky A, Eun LY, Hall TL, Tran BC, Fowlkes JB, Cain CA. Controlled ultrasound tissue erosion. IEEE Trans Ultrason Ferroelectr Freq Control. 2004; 51:726–36. [PubMed: 15244286]

Zhang X, Miller RM, Lin KW, Levin AM, Owens GE, Gurm HS, Cain CA, Xu Z. Real-time feedback of histotripsy thrombolysis using bubble-induced color Doppler. Ultrasound Med Biol. 2015; 41:1386–401. [PubMed: 25623821]

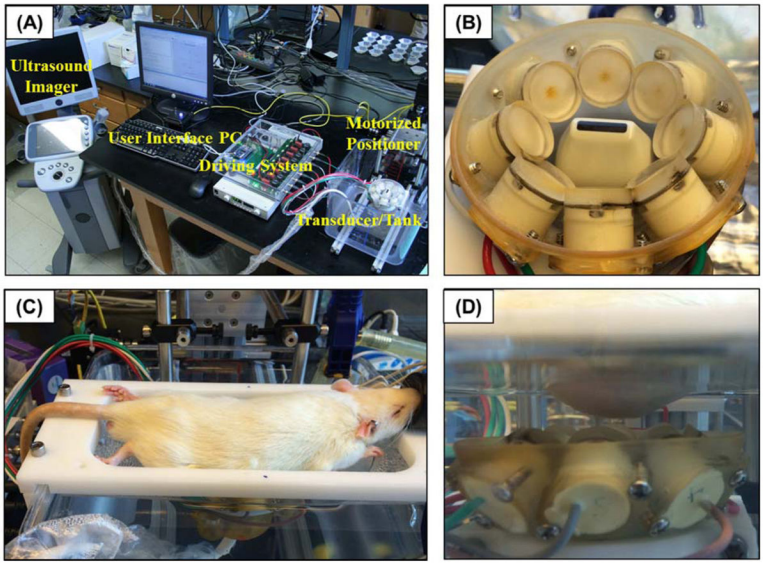

Figure 1. Histotripsy *in vivo* rat liver ablation experimental setup

(A) A 1 MHz histotripsy therapy transducer with coaxially aligned ultrasound imaging probe was attached to a motorized 3D positioning system controlled using a PC console. **(B)** The histotripsy transducer consisted of 8 transducer elements in a ring with the imaging probe inserted in the center. **(C)** For treatment, an anesthetized rat was placed on a stage above the histotripsy transducer. **(D)** The transducer was placed inside a tank of degassed water beneath the anesthetized rat, and histotripsy was noninvasively applied to the liver through the intact abdomen.

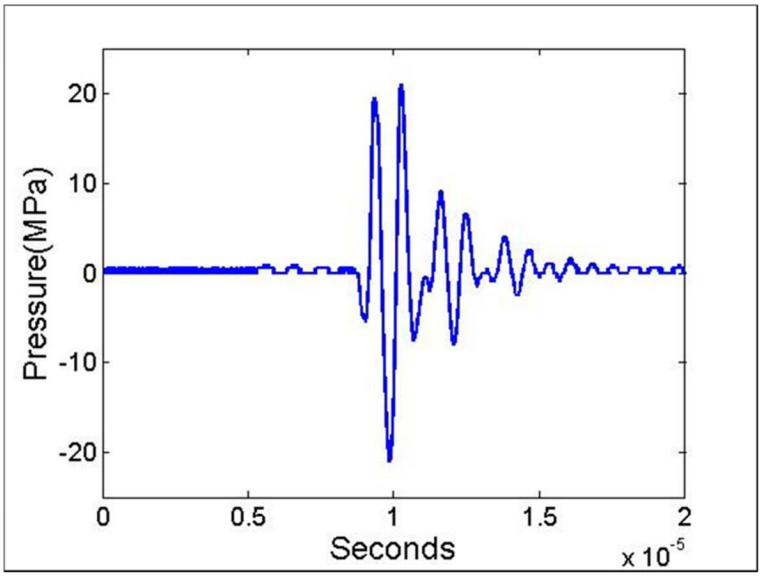

Figure 2. Acoustic waveform

Image shows an example acoustic waveform generated by the 8-element 1 MHz histotripsy small animal transducer and measured by the FOPH.

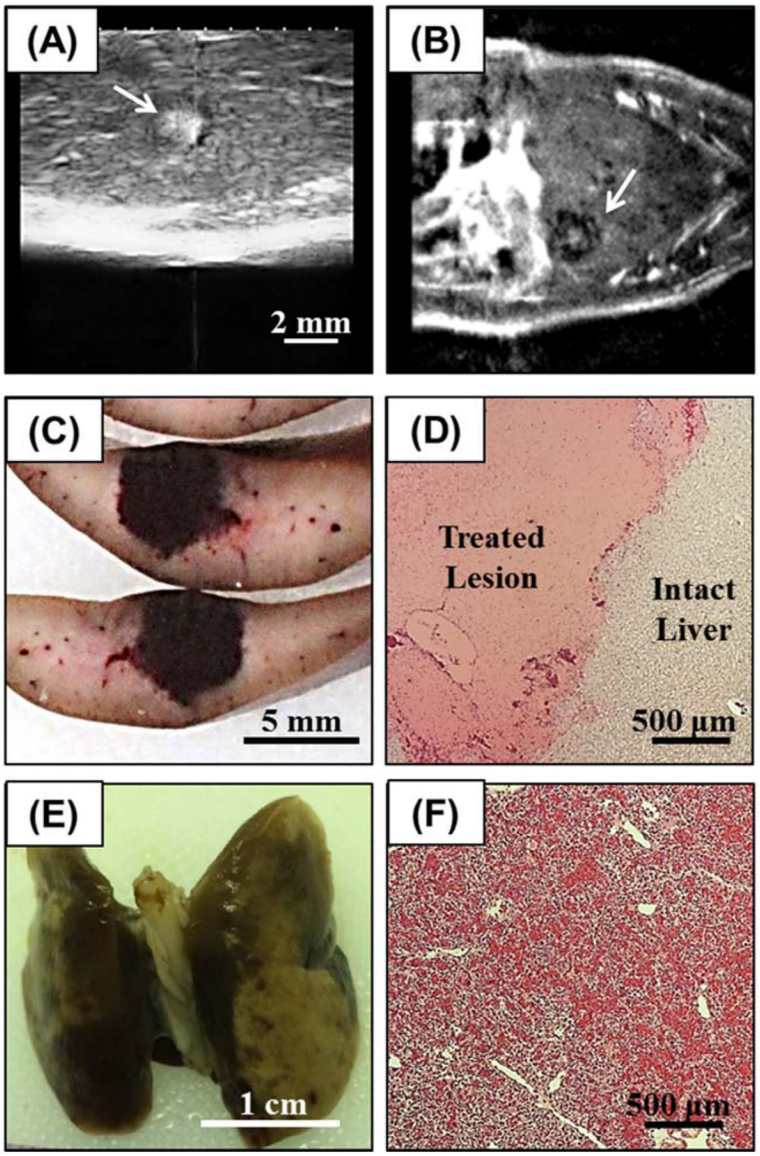

Figure 3.

(A) Histotripsy treatments were applied to the rat liver guided by real-time ultrasound imaging (arrow indicates histotripsy bubble cloud). After treatment, liver lesions were assessed using **(B)** MRI (lesion indicated by arrow), followed by assessment with **(C)** gross morphology and **(D)** histology. In addition to the liver, the inferior lobes of the lungs were harvested after treatment and assessed using **(E)** gross morphology and **(F)** histology.

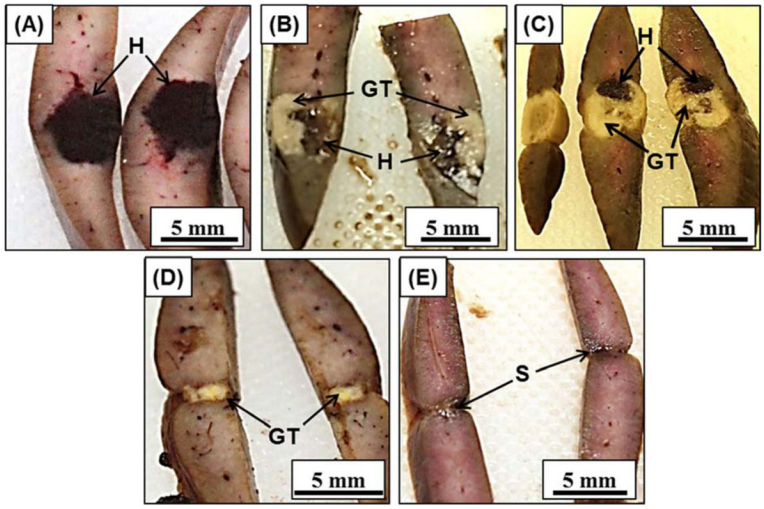

Figure 4.

Histotripsy liver lesions were assessed for gross morphology after animals were sacrificed on days 0, 3, 7, 14, 28 **(A–E)**. Darkly colored hematomas seen on **(A)** day 0 were replaced with granulation tissue on **(B)** day 3 and **(C)** day 7. The granulation tissue was mostly replaced by regenerated liver parenchyma on **(D)** day 14 and **(E)** day 28, leaving a small contracted scar. H=hematoma, GT=granulation tissue, S=scar

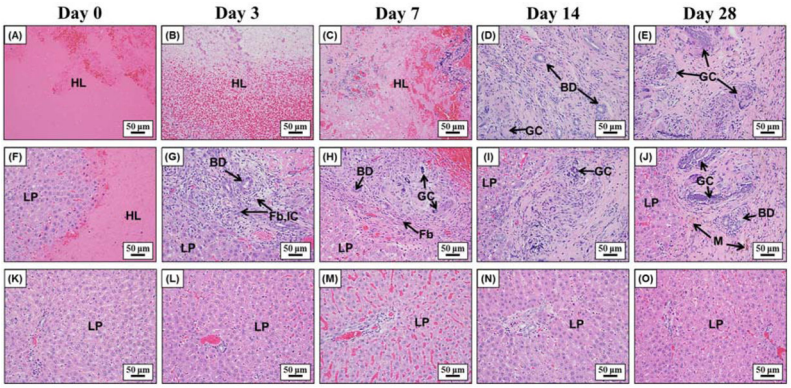

Figure 5.

Representative histology images showing the center of the lesion **(top row)**, the lesion interface **(middle row)**, and the surrounding liver parenchyma **(bottom row)** after day 0, 3, 7, 14, and 28. Initially, lesions were almost solely composed of extravasated red blood cells and fibrin on day 0 **(A, F)**. Fibroblasts started to grow into the lesion from the interface together with inflammatory cells and foci of bile ductular proliferation at day 3 **(G)** and day 7 **(H)**. At day 14 **(D, I)** and day 28 **(E, J)**, the majority of the lesion was replaced by regenerated liver parenchyma with only a small focus of residual scar and foreign body giant cells with calcified undigested debris in their cytoplasm. The surrounding liver parenchyma is unremarkable with no significant inflammation, necrosis, or fibrosis **(K–O)**. LP=liver parenchyma, HL=histotripsy lesion, BD=bile ducts, Fb=fibroblasts, IC= inflammatory cells, M=macrophages, GC=giant cells.

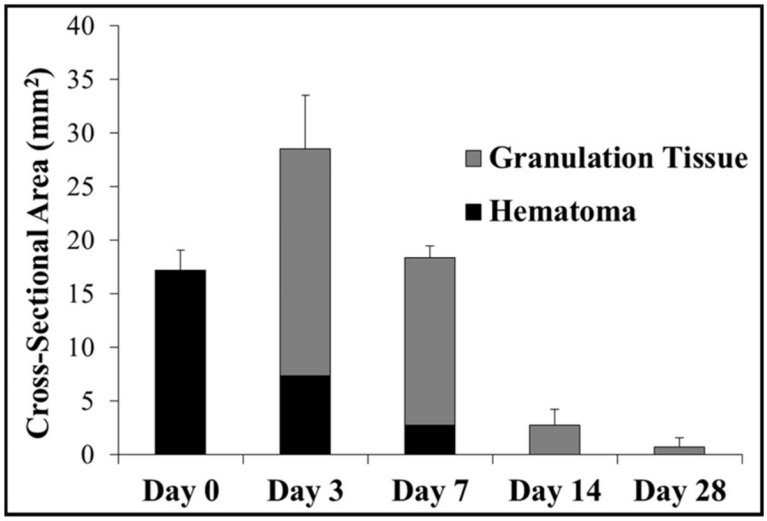

Figure 6.

Plot shows the average maximum cross-sectional area of the histotripsy liver lesions measured over the course of the experiment. The area of the hematoma and granulation tissue components of the lesion, as well as the total lesion cross-sectional area, were compared for rats euthanized after day 0, 3, 7, 14, and 28. Following an increase in the maximum cross-sectional area between day 0 and 3, there was a rapid reduction in lesion size over the remainder of the study. All differences in lesion size were significant ($p<0.05$).

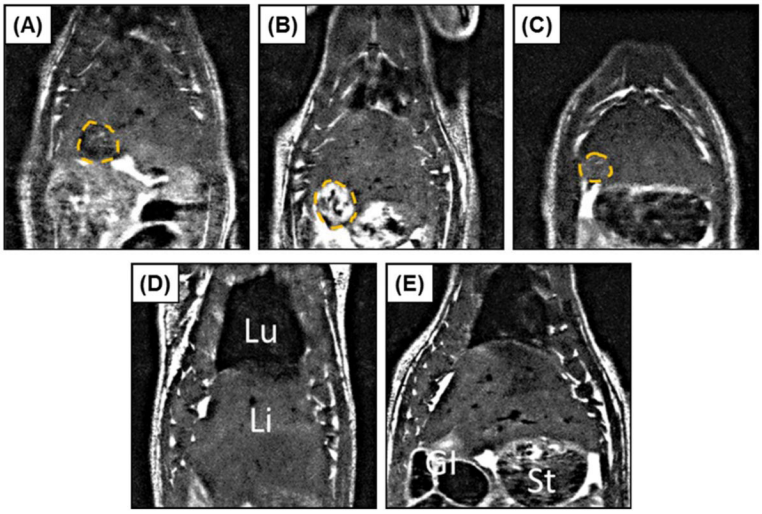

Figure 7.

Representative MRI images for one rat acquired on days 0, 3, 7, 14, and 28 **(A–E)**, illustrating approximately the maximum cross-sectional area of the histotripsy lesion (Lesion=dashed orange line; Lu=lungs, Li=liver, St=stomach, GI=gastrointestinal tract). Lesions showed primarily negative contrast on day 0 **(A)** and positive contrast on day 3 **(B)**. Signal intensity rapidly normalized at later time points **(C–E)**, with no lesion quantifiable in any animal by day 28 **(E)**.

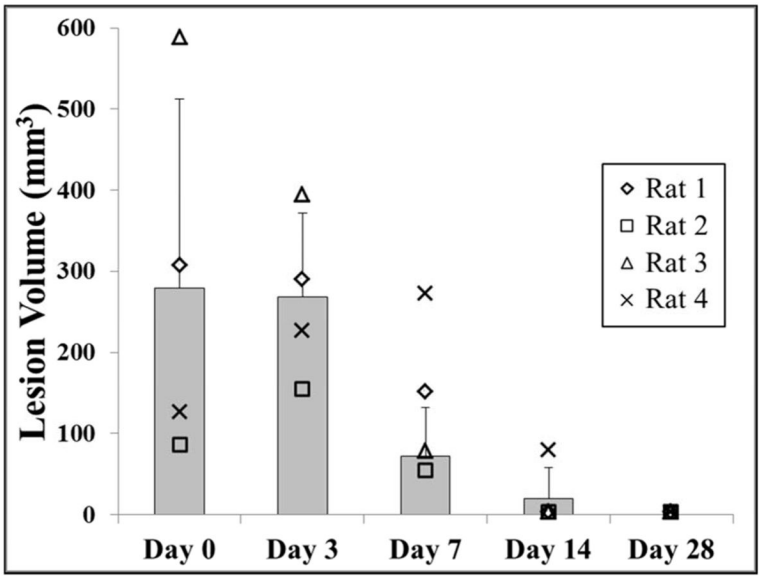

Figure 8.

Plot shows the lesion volume measured by MRI for rats euthanized after day 28 (n=4). No significant difference in lesion size was observed between day 0 and day 3 ($p>0.05$). After day 3, there was a significant decrease in lesion volume over the remainder of the study ($p<0.05$) with no quantifiable lesions observed after day 28.

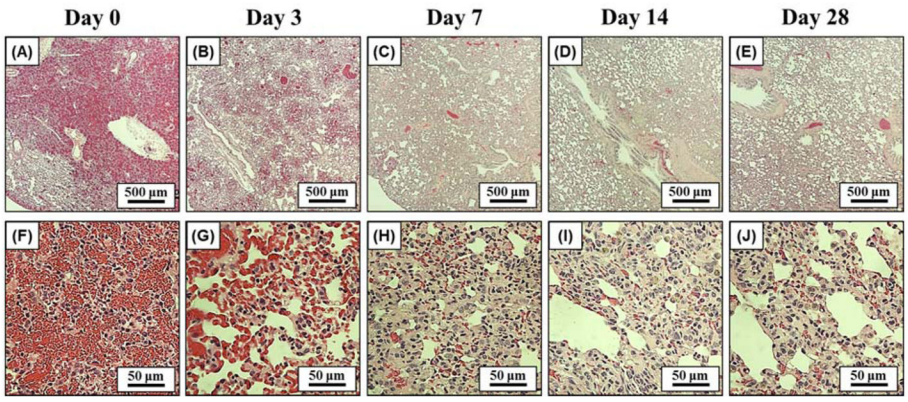

Figure 9. Lung Histology

Histology images of the inferior lobes of the lung after days 0, 3, 7, 14, 28 using 4x **(A–E)** and 40x magnification **(F–J)**. Results showed localized lung hemorrhage on day 0 **(A, F)**, indicated by the presence of red blood cells throughout the alveolar space. After recovery from therapy, the number of red blood cells inside the alveolar space steadily decreased, with minimal hemorrhage remaining after day 28 **(E, J)**.